

Controlling the stereochemistry and regularity of butanethiol self-assembled monolayers on Au(111)

Jiawei Yan^{1,2}, Runhai Ouyang³, Palle S. Jensen¹, Erhad Ascic¹, David Tanner¹, Bingwei Mao², Jingdong Zhang,¹ Chunguang Tang,³ Noel S. Hush,^{3,4} Jens Ulstrup,^{*1} and Jeffrey R. Reimers^{*5,6}

¹ Department of Chemistry, Technical University of Denmark, Kongens Lyngby 2800, Denmark

² State Key Laboratory for Physical Chemistry of Solid Surfaces, and Department of Chemistry, College of Chemistry and Chemical Engineering, Xiamen University, Xiamen, Fujian 361005, China

³ School of Chemistry F11, The University of Sydney, NSW 2006 Australia

⁴ School of Molecular Bioscience, The University of Sydney, NSW 2006 Australia

⁵ International Centre for Quantum Molecular Structure, College of Science, Shanghai University, Shanghai 200444, China.

⁶ School of Physics and Advanced Materials, The University of Technology Sydney, Sydney NSW 2007 Australia.

Supporting Information Placeholder

ABSTRACT. The rich stereochemistry of the self-assembled monolayers (SAMs) of the four butanethiols on Au(111) is described, SAMs containing up to 12 individual C, S, or Au chiral centers per surface unit cell. This is facilitated by synthesis of enantiomerically pure 2-butanethiol (the smallest unsubstituted chiral alkanethiol), followed by in situ scanning tunneling microscopy (STM) imaging combined with density-functional theory (DFT) molecular dynamics STM-image simulations. Even though butanethiol SAMs manifest strong head-group interactions, steric interactions are shown to dominate SAM structure and chirality. Indeed, steric interactions are shown to dictate the nature of the head-group itself: whether it takes on the adatom-bound motif $RS^*Au(0)S^*R$ or else involves direct binding of RS^* to face-centered cubic (FCC) or hexagonal close-packed (HCP) sites. Binding as RS^* produces large organizationally chiral domains even when R is achiral, while adatom binding leads to rectangular plane groups that suppress long-range expression of chirality. Binding as RS^* also inhibits the pitting intrinsically associated with adatom binding, desirably producing more regularly structured SAMs.

1. Introduction

The formation of self-assembled monolayers (SAMs) of small molecules offers unique insight into the interactions between head-group forces, substrate-relaxation forces, and intermolecular steric interactions in the manifestation of surface chirality. Surface chirality can manifest if the adsorbate molecules are themselves chiral, if the atomic structures formed at the interface are chiral, or if the macroscopic arrangement of adsorbate molecules is chiral,¹⁻⁶ and indeed all effects may operate concurrently, leading to complex surface stereochemistry. Chiral surfaces, no mat-

ter by what means they are formed, are of general interest for chiral resolution⁷⁻⁸ and catalysis.⁹⁻¹¹ Control of chirality could also be critical to any single-molecule device assembled on a surface. Often large molecules are preferred for consideration as the steric repulsions and intermolecular attractions stemming from their geometric structure typically serve to control the monolayer plane group. This is what leads to the observed propensity of plane groups embodying 2-fold rotations in packing motifs, groups that do not intrinsically destroy global chirality.^{2,5} Hence most SAMs pack into chiral structures, in contrast to most crystals for which the same steric packing forces lead to a preference for centrosymmetric arrangements that are intrinsically achiral. However, when the molecules become small enough so that steric interactions no longer obviously control the structure, the head-group interaction could dominate to control SAM chirality.

Here we describe the chirality properties of the SAMs formed by the butanethiols (Chart 1), a family of adsorbate molecules that

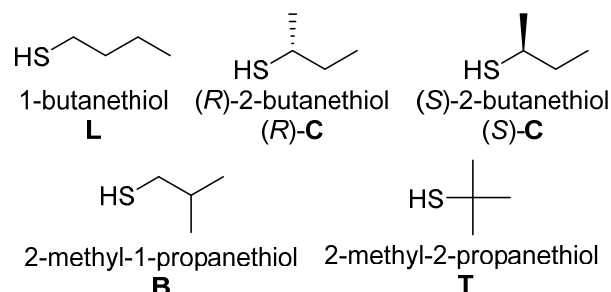


Chart 1. The butanethiol family.

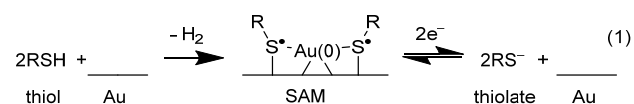
includes the smallest unsubstituted chiral alkanethiol, 2-butanethiol. We analyse established structural properties for SAMs of the linear isomer 1-butaneethiol **L**,¹²⁻¹⁴ the branched achiral isomer 2-methyl-1-propaneethiol **B**,¹⁵⁻¹⁶ the tertiary isomer

2-methyl-2-propanethiol **T**,^{15,17} and a racemic mixture¹⁸ **R** of the enantiomer forms (*R*)-**C** and (*S*)-**C** of 2-butanethiol. In addition, we present the in-situ synthesis of the pure *R* and *S* enantiomeric forms of 2-butanethiol, their observed in-situ scanning-tunneling microscopy (STM) images on Au(111) in solution at room temperature under electrochemical control, and STM image simulations based on extensive conformational searching and molecular dynamics simulations using density-functional theory (DFT). Assignment is also made for the structure of the minor low-density phase observed in SAMs of **R**.

The focus of this work is determination of the nature of the head group and its chirality. On gold nanoparticles¹⁹ and on gold surfaces, adatom-bound head-group motifs²⁰⁻²² $RS^*Au(0)S^*R$ (or its oligomerized variants)²² are commonly found.⁸ Another observed motif on both nanoparticles²³ and surfaces^{17-18,24} involves direct binding of RS^* to Au(111) face-centered cubic (FCC) or hexagonal-close-packed (HCP) sites,²⁵⁻²⁷ normally disfavored on nanoparticles because of their greater curvature²⁸ but occupied whenever steric or packing interactions or tail-group Coulombic interactions prevent $RS^*Au(0)S^*R$ formation.¹⁴ Another often considered possible alternative is bonding via $RS^*Au(0)$.²⁹⁻³¹

Some unusual features of our experimental approach are critical to the determination of the structure of the SAMs of enantiomerically pure 2-butanethiol. Gold pits and gold islands form in the SAMs³²⁻³³ that we manipulate under in-situ electrochemical control. By using single-crystal gold substrates containing very large flat terraces so large that gold cannot be transported from surface edges to provide adatoms, we measure the concentration of gold atoms per surface cell, providing vital composition information.

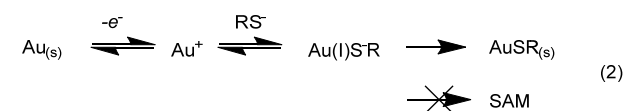
Another essential feature is the electrochemical production of alkanethiolates. These anionic species as such do not bind to gold³⁴⁻³⁶ and when formed in situ result in the immediate reductive desorption of SAMs.³⁶⁻³⁸ SAM production from thiols is irreversible^{36,39-40} and we achieve SAM assembly and destruction using the reactions:



This may appear confusing as often the label “thiolate” is applied to describe sulfur-bound SAMs to gold regardless of the actual chemical form of the sulfur. However, all aspects of the chemical and spectroscopic properties of these SAMs are controlled by the actual oxidation states of the SAM components. All DFT calculations of gold-sulfur surfaces^{27-28,41-45} indicate that the filled Au *d* band interacts with half-occupied *S p* orbitals for which the two feasible valence descriptions are a non-bonding thiol and neutral gold structure $RS^*Au(0)S^*R$ and an ionically bonded Au(I)-thiolate structure $RS^*Au(I)S^*R$. Allowed charge polarization effects can add covalent bonding character to both the $RS^*Au(0)S^*R$ and $RS^*Au(I)S^*R$ structures. DFT calculations,^{27-28,41-45} including those that treat dispersion accurately,⁴⁶ indicate that the structure is polarized $RS^*Au(0)S^*R$. A wide range of direct experimental measurements verify this picture.^{39,42-43,47-53} Further, near-edge X-ray absorption fine structure (NEXAFS) measurements⁴⁴ of SAMs directly reveal a critical low-energy *unoccupied* orbital to be one consistent only with $RS^*Au(0)S^*R$ as this orbital would be *occupied* in the thiolate.

Whilst a basic understanding of the chemistry of gold-sulfur interfaces is critical to the experiments that we perform subjecting

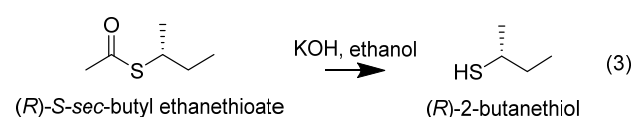
pre-prepared SAMs to reductive stress, it is also required to understand the effects of oxidative stress. Exposing a gold surface under such conditions would facilitate pre-preparation of Au(I) where it can be mixed with pre-prepared thiolates RS^* in solution. This process *does not* result in SAM protection, however. Instead, the surface is etched to form Au(I)-thiolate films.³⁴



By analogy, if Au(I) S^*R type species formed during nanoparticle growth, they would be expected to destroy the nanoparticles, converting them into analogous molecular films; indeed, it is known that thiolate pre-preparation must be inhibited during the reduction of Au(III) salts to form nanoparticles,^{36,54} whilst much weaker reducing agents such as thiols can play a critical role.^{36,55} Incorrect description of the nature of S and Au in nanoparticles leads to incorrect descriptions of the chemistry of nanoparticle structure and formation.²⁷⁻²⁸

2. Experimental and Computational Methods

The synthetic strategy adopted for formation of the SAMs of enantiomerically pure 2-butanethiol was to first synthesize and characterize (*R*)-*S*-*sec*-butyl ethanethioate and (*S*)-*S*-*sec*-butyl ethanethioate using the stereospecific synthesis of Volante,⁵⁶ full details and characterization data are provided in the Supporting Information (SI) Sects. S1-S2. An excess of these molecules were then converted in situ to their thiol forms by base hydrolysis in ethanol, e.g.,



and left to soak a freshly annealed Au(111) single-crystal substrate for 12 hours. This was then washed first with ethanol and then with Millipore water before immersion in a 20 mM KH_2PO_4 solution for STM measurement, see SI Sect. S3. Details of the STM conditions and voltammetry are also given in the SI.

DFT calculations were performed using the PW91 density functional⁵⁷ corrected⁵⁸ for dispersion using the D3 method⁵⁹ in the VASP package.⁶⁰ Default energy cutoffs defining the number of plane-waves in the basis set are used. Full details including *K*-point sampling are described in detail in the SI. Time-averaged STM images were obtained by analyzing configurations extracted from 300 K DFT molecular dynamics simulations using the Tersoff-Hamann approximation⁶¹ at a bias voltage of 0.5 V.

3. Results.

a. STM images of the enantiomerically pure 2-butanethiols and SAM observation. The STM images of both SAMs indicate assembly into the $(4 \times \sqrt{3})-2$ lattice, see Fig. 1 and SI Sect. S4. The presence of two molecules per unit cell was confirmed by reductive desorption experiments (see SI Sect. S6) depicting sharp desorption peaks at -0.816 ± 0.01 and -0.818 ± 0.01 V vs. saturated calomel electrode (SCE), the areas of which indicate adsorbate coverages of $6.2 \pm 0.4 \times 10^{-10}$ mol cm^{-2} and of $6.4 \pm 0.4 \times 10^{-10}$ mol

cm^{-2} for (*S*)-2-butanethiol and (*R*)-2-butanethiol, respectively, close to the anticipated value for 2 molecules per cell of 5.8×10^{-10} mol cm^{-2} . The adsorbate coverage is therefore 25%. Repetition of this procedure using a 50:50 mixture of the *S*-*sec*-butyl ethanethioate enantiomers yields a higher-density SAM indistinguishable from that determined previously¹⁸ using commercial racemic 2-butanethiol adsorbate.

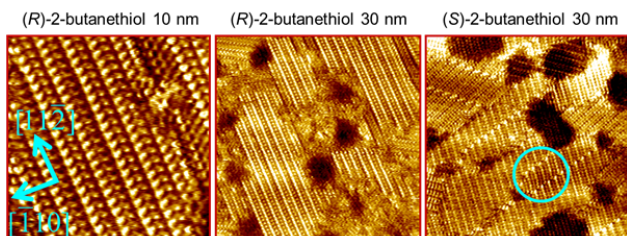


Fig. 1. STM images of SAMs of chemisorbed (*R*)-2-butanethiol (tunneling current $I_t = 0.04$ nA, bias voltage $V_{\text{bias}} = 0.10$ V) and (*S*)-2-butanethiol ($I_t = 0.08$ nA and $V_{\text{bias}} = 0.40$ V). The blue circle highlights two domain boundaries.

Images of the *R* stereoisomer were obtained at length scales down to $10 \text{ nm} \times 10 \text{ nm}$ whereas only $30 \text{ nm} \times 30 \text{ nm}$ images were stable for *S*. These images clearly show two spots per surface cell with one brighter than the other, plus a darker region. Although the SAMs show global point chirality, they assemble into rectangular unit cell with nearly co-linear internal structural features, minimizing visualization of long-range manifestations of chirality. Domain boundaries between possibly mirror-image forms can be found, however, as highlighted in the figure.

The larger-area scans in Fig. 1 show the presence of disordered regions, which in places cover up to $\sim 15\%$ of the surface, and also pitted regions of the surface. Supporting Information Sect. S5 analyses some larger-area scans, identifying the pits as covering ca. 10% of the surface. Pits are formed when adatoms are mined, and as large terraces are used to prevent mining from step edges and also as in these experiments the gold ($22 \times \sqrt{3}$) reconstruction is lifted *before* SAM formation, all adatoms must come from pits. Because the $(4 \times \sqrt{3}) - 2$ lattice contains 10 gold atoms per layer, a 10% pit coverage therefore implies the presence of one additional gold atom per cell. SAMs may also contain local vacancies in the top gold layer,^{22,62-64} so the observed pit coverage could be accounted for by atomic structures containing per cell either one adatom and no local vacancy (1A0V) or else two adatoms and one vacancy (2A1V).

b. DFT simulation of STM images of enantiomerically pure 2-butanethiol SAMs. With 2 adsorbate molecules per surface cell, the observed SAMs possess a significant configuration space of possible atomic structures. To process this, two classes of geometric variables controlling the structure were identified: (1) chemical descriptors specifying the locations of the gold and sulfur atoms, and (2) three torsional angles (Au-S, S-C, and C-C) per adsorbate specifying conformational details. We considered all known possible sulfur arrangements explicitly, and for each of these scanned the torsional-angle spaces using a product grid search involving the examination of ca. 10^5 possible structures. These were pre-screened by selecting only 100-200 structures with non-bonded C-C distances in excess of 3.2 Å for which DFT optimizations were then run. All calculations were constrained to the observed $(4 \times \sqrt{3}) - 2$ substrate lattice but the number of gold atoms and surface vacancies were varied.

Four stable chemical structures depicting the gold and sulfur head-group atoms were identified, all containing gold adatoms bound to two sulfur atoms and the surface. Structures with adsorbate molecules bound directly to the Au(111) surface relaxed to spontaneously lift an adatom off the surface to make a local vacancy, while structures in which a gold adatom was bound to just a single sulfur atom led to polymerization. The four stable chemical structures are shown in Fig. 2 and are denoted H (horizontal), L (left), R (right), and T (top) after the location of the gold adatoms with respect to the substrate (see SI Fig. S7). Stable conformers were always found for the two gauche arrangements G_+ and G_- as well as for the higher-energy anti conformer A of the C-C torsion of each adsorbate molecule. For the L and R species, all other torsional variables were found to be tightly coupled, leading to only two stable molecular configurations. These may be effectively characterized based on the involved C-S torsional angles: in one case both adsorbate molecules have their ethyl groups erecting vertically from the surface, *uu*, (structures named L_{uu} and R_{uu}) and in the other case one erects while one is oriented in the surface plane, *ud*, (named $L_{ud} \equiv L_{du}$ and $R_{ud} \equiv R_{du}$). Hence a total of 6 stable structural types were found. The calculated energies for all 9 possible C-C conformers of these are given in SI Sect. S7a whilst the lowest-energy structure of each type is shown in Fig. 2. Summarizing the results, a set of empirical rules depicting low-energy structures is developed in SI Sect. S7b.

Shown on the top row of Fig. 2 are sketches depicting each structure's geometry and chirality. Every atom in the C-S-Au-S-C central unit can take on enantiomeric forms, indicated in the figure by shading (*S* is black, *R* is grey, achiral is white). Fig. 2 applies only to (*R*)-2-butanethiol SAMs and so all end units in this figure are shaded grey; analogous structures for (*S*)-2-butanethiol SAMs may be obtained simply by reflection, interchanging all stereocenters (see SI Sect. S7a). For the gold adatom, the L site is *S* while the R site is *R* and the H and T sites are achiral. The sulfur atoms may take on either enantiomeric form, however, controlling the overall molecular shape,⁶ only *RR* or *SS* sulfur configurations appear in Fig. 2, indicating that all adatom motifs take on a syn (often called *cis*)^{6,63} structure. The *SR* and *RS* sulfur configurations are known for **B** and **R**, however,^{15-16,18,63} producing anti (often called *trans*)^{6,63} structures.

The lowest-energy structure is found to be L_{uu} , but R_{ud} is only $\Delta E = 0.08$ eV higher; this difference is below the accuracy of the method and of the order of likely entropy corrections to the Gibbs free energy. At $\Delta E = 0.16$ eV, R_{uu} may also be feasible, but the L_{du} and T structures are unlikely, having $\Delta E = 0.24$ eV, while H is of very high energy at $\Delta E = 2.03$ eV.

The T structure has the gold adatoms sitting vertically above a gold surface atom instead of being at a bridge site. Indeed, all other structures utilize one of the three (L, R, H) bridge sites, see SI Fig. S7. For achiral adsorbates the L and R sites are equivalent but chiral adsorbates discriminate between them. The high-energy H structure assembles the adsorbate molecules into two parallel infinite chains per surface cell of the form -S-Au-S-Au-S. As such, this structure includes two adatoms per surface cell and is consistent with the observed pit coverage there must also be one local vacancy per cell (2A1V). However, we find for all 6 structural types shown in Fig. 2, formation of pits from local gold surface vacancies is considerably exothermic by of order 2 eV, in contrast to the -0.20 to 0.04 eV energy differences found for the other butanethiols.⁶³ Structure T is thus predicted to have 2 adatoms and no vacancies (2A0V) and hence be inconsistent with the experimental data. The other five structures all have one adatom and no vacancy (1A0V) and are therefore consistent with it.

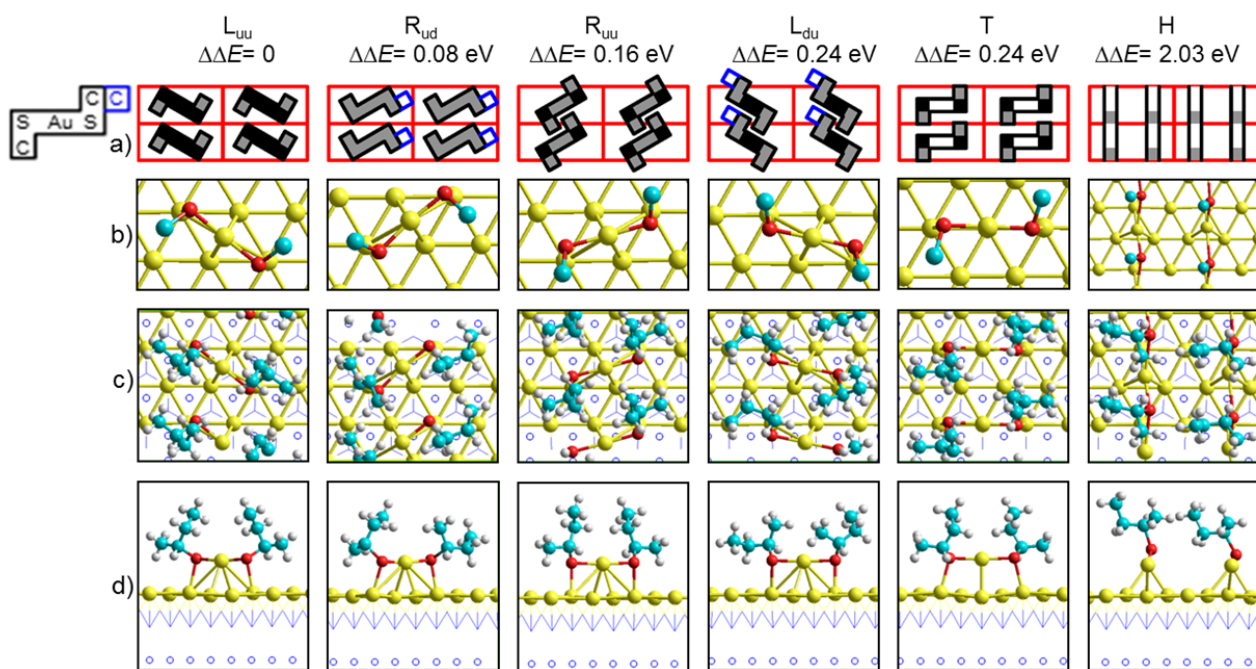


Fig. 2. Four copies of DFT optimized structures and energies depicting the observed SAMs of (*R*)-2-butanethiol on Au(111). Rows b) and c) show top views of the SAM, restricted to just the surface gold layer and a single C-S-Au-S-C unit in b); sulfur (red), carbon (cyan), hydrogen (white), gold top layer and adatoms (yellow), gold subsurface layer (blue bond to top layer), gold 3rd layer (blue open circles), gold fourth layer not shown. Row d) shows the side view corresponding to row c). Row a) shows characteratures of row b), highlighting the stereochemistry at the C-S-Au-S-C centers: *R* (gray), *S* (black), or achiral (white), whilst blue squares indicate flat lying ethyl groups.

To investigate effects of thermal motion manifest on a short time scale,^{14,16,21-22,65-66} DFT molecular dynamics (MD) simulations at 300 K were performed for each of the 9 conformations of the L_{uu} structure obtained by rotating about the C-C torsion angles. The resulting torsional-angle probability distributions (see SI Sect. S7c) reveals that only three of the forms are stable on the 10 ps timescale. The nudged electing band (NEB) method was then applied to find transition-state energies linking these three structures, evaluated to be 0.3 eV for a concerted transition state. While transformations between structures will proceed sequentially, this small concerted-reaction barrier clearly indicates that the interconversion of all structures will happen on the 1 m STM timescale. The STM image of L_{uu} is therefore predicted to be symmetric, inconsistent with the bright-spot dull-spot observed pattern.

Structure L_{ud} is intrinsically asymmetric, however, owing to one adsorbate molecule having an ethyl group oriented vertically whilst the other is horizontal, see Fig. 1. Molecular-dynamics simulations on the 10 ps timescale induces only local motions in this densely packed structure and the calculated STM image varies little and is in good agreement with the observed image, as shown in Fig. 3. It appears that the observed structure is indeed L_{ud} . In previous studies of butanethiol SAMs, the calculated structure of second-lowest energy was sometimes also found to only be consistent with the observed STM image,⁶³ but the largest error previously found was 0.03 eV compared to 0.08 eV here.

However, the alternate domain of structure R_{du} would have the same energy as R_{ud} and hence there must be no equilibration on the STM timescale. Indeed, the appearance of two symmetrically related domains can be seen in the zoomed-out images in Fig. 1 which show fault lines in the images across which the bright-spots and dull-spots interchange. Equilibration of asymmetric variants of the L_{uu} structure was predicted to be very rapid as it involved

only uncoupled local motions on each individual adsorbate molecule. However, tilting the ethyl groups downwards introduces a strong interaction between adsorbate molecules on adjacent adatoms, with for example global structures of the form R_{dd} not allowed. Therefore the first step in any interchange process must be the conversion of R_{ud} to R_{uu} which from SI Table S1 is endothermic by 0.1 to 0.2 eV. As the calculations appear to underestimate the energy of L_{uu} compared to R_{ud} by at least 0.08 eV, this energy cost may indeed be significantly higher. Such an interchange allows a neighbouring adatom complex to change from R_{ud} to R_{du} (see SI Sect. S7d) at a significant energy cost, but the effect is local and any subsequent change requires still more energy. Chemical structure variations in the centre of domains are thus prevented. Variations could be initiated at domain boundaries but their propagation would still involve an energy cost. A variety of trial calculations reported in SI Sect S7d qualitatively support the hypothesis that the R_{ud} structure is locked.

c. DFT simulation of STM images of the low-density phase of racemic 2-butanethiol SAMs. SAMs produced from racemic mixtures of the two 2-butanethiols have previously been studied,¹⁸ revealing a major phase R_{30} consisting of a $(10 \times \sqrt{3}) - 6$ domain (30% coverage) with near pg symmetry. The chirality and structure of its six adsorbate molecules per cell were assigned as “(SR)R(RS)S”, meaning in order: “(SR)” one *S* and one *R* adsorbate on an adatom, “R” one *R* adsorbate molecule on a FCC Au(111) site, “(RS)” one *R* and one *S* adsorbate on an adatom, and finally “S” one *S* adsorbate on a HCP lattice site. In this notation, the SAMs of the previously considered chirally resolved molecules are described as being either (*RR*) or (*SS*). However, an unassigned minor domain R_{25} was also observed for SAMs made from the racemate of the form $(8 \times \sqrt{3}) - 4$ (25% coverage)

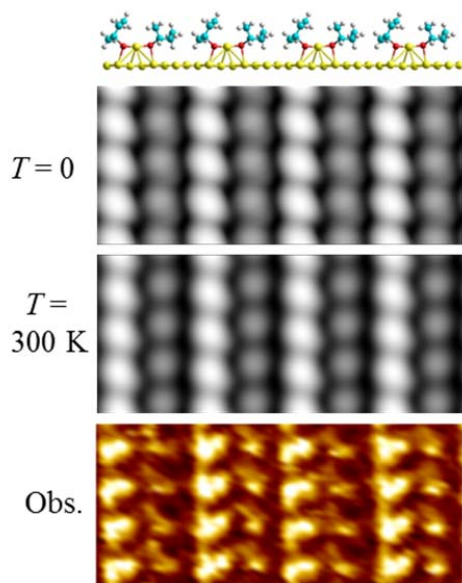


Fig. 3. SAM of (*R*)-2-butanethiol on Au(111) showing a 4×4 grid of $(4 \times \sqrt{3}) - 2$ surface cells: (top) simulated STM image at 0 K and associated atomic structure R_{ud} , (middle) simulated STM image for R_{ud} following 10 ps molecular dynamics at 300 K, and (bottom) observed image; sulfur (red), carbon (cyan), hydrogen (white), gold (yellow).

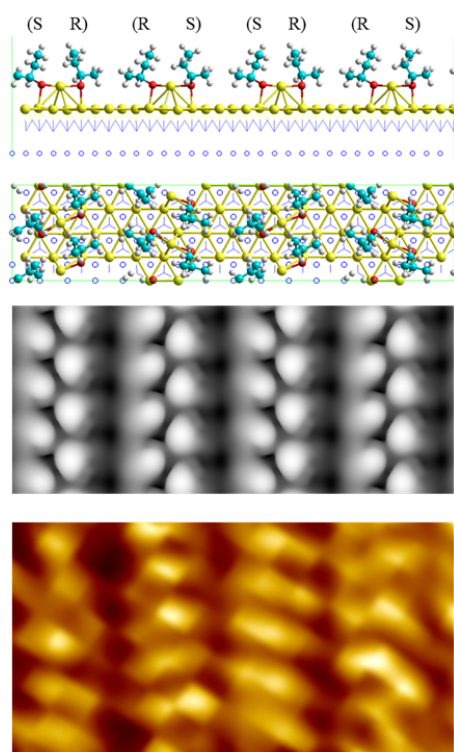


Fig. 4. SAMs from a racemic mixture of the 2-butanethiols on Au(111) showing 4×4 surface cells: (top) simulated STM image at 0 K and associated atomic structure of (*SR*)(*RS*) chirality, and (bottom) observed image for the $(8 \times \sqrt{3}) - 4$ phase; sulfur (red), carbon (cyan), hydrogen (white), gold top layer and adatoms (yellow), gold subsurface layer (blue bond to top layer), gold 3rd layer (blue open circles), gold fourth layer not shown.

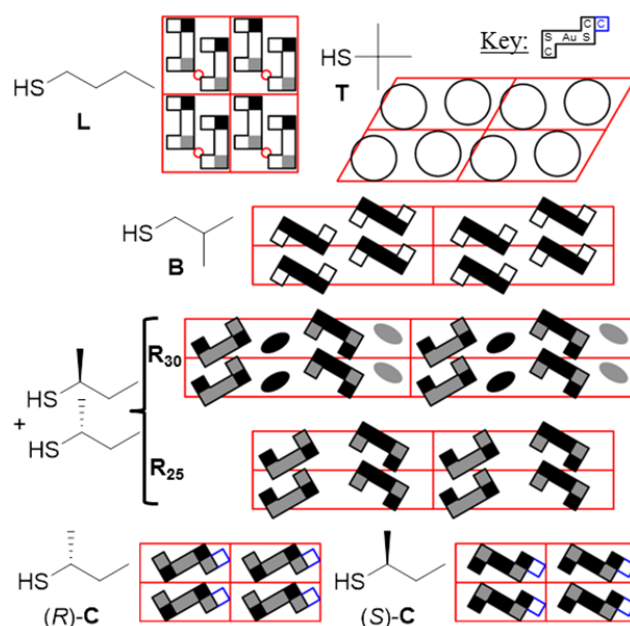


Fig. 5. Sketches of four replicas of the surface cells of single domains within the butanethiol SAMs on Au(111), see Table 1. Black square and rectangular shapes depict the structure and chirality of C-S-Au-S-C units (see key) while circular and elliptical shapes depict adsorbates directly bound to Au(111) and blue squares indicate horizontally oriented ethyl groups. Shaded regions indicate either *R* (gray), *S* (black), or achiral (white) carbon, sulfur, or gold-adatom centers. Red circles indicate local vacancies.

with pg symmetry. Application of the methods developed herein for the chirally resolved SAMs to this structure yield two possibilities of form (*SR*)(*RS*) and (*RS*)(*RS*). Of these, (*SR*)(*RS*) is lower in energy by 0.03 eV and has the observed pg symmetry whereas (*RS*)(*RS*) only has $p1$ symmetry and leads to a calculated STM image quite different from that observed. The calculated (*SR*)(*RS*) structure is given in Fig. 4 where its calculated STM image at 0 K is shown to be in good agreement with the observed¹⁸ image. An alternative possibility for a SAM at 25% coverage is that it forms into separate $(4 \times \sqrt{3}) - 2$ $p1$ domains of individual characters (*RR*) and (*SS*), involving spontaneous chiral resolution of the racemate. We calculate the energies of such domains to be 0.03 eV higher than that of the (*SR*)(*RS*) domain.

4. Discussion: Chirality of the butanethiol SAMs on Au(111)

Table 1 indicates that the butanethiol isomers all show different surface-cell lattices, as dictated by their different steric interactions, very different head-group arrangements, and very different chirality properties; sketches of these properties are shown in Fig. 5. The head-group properties are indeed widely varied, embracing both syn and anti adatom motifs as well as sulfur groups bound directly onto both Au(111) FCC and HCP sites (indicated by circles and ellipses in Fig. 4). Also, the head-group interaction sometimes involves local vacancy formation. In general, the energetics controlling the head-group pattern are delicately balanced,⁶³ allowing steric interactions to modulate substrate relaxation effects to in effect control the whole assembly process.

Table 1. Chirality properties of the butanethiol SAMs on Au(111).

butanethiol isomer	Cov.	Lattice	Plane group	Adatom / Vac.	Head group(s)	Carbon chirality	Sulfur chirality	Point chirality	Chiral domains
linear L	1/3	$(3 \times 2\sqrt{3}) - 4$	$p1 \sim cm$	2A1V	2 × adatom syn	achiral	2 × <i>RS</i>	local	unclear
branched B	1/4	$(8 \times \sqrt{3}) - 4$	$p1 \sim p2$	2A0V	2 × adatom anti	achiral	2 × <i>RR</i> or <i>SS</i>	local	subtle
tertiary T	1/7	$(2\sqrt{7} \times \sqrt{7}) - 2$	$p1$	0A0V	2 × FCC site	achiral	-	local	distinct
chiral R ₃₀	3/10	$(10 \times \sqrt{3}) - 6$	$\sim pg$	2A0V	2 × adatom syn, 1 × FCC, 1 × HCP	3 <i>R</i> and 3 <i>S</i>	2 × <i>RS</i>	local	no
chiral R ₂₅	1/4	$(8 \times \sqrt{3}) - 4$	pg	4A0V	2 × adatom syn	2 <i>R</i> and 2 <i>S</i>	2 × <i>RS</i>	local	no
chiral (<i>R</i>)- C	1/4	$(4 \times \sqrt{3}) - 2$	$p1 \sim p2$	1A0V	1 × adatom anti	2 <i>R</i>	<i>SS</i>	global	subtle
chiral (<i>S</i>)- C	1/4	$(4 \times \sqrt{3}) - 2$	$p1 \sim p2$	1A0V	1 × adatom anti	2 <i>S</i>	<i>RR</i>	global	subtle

Isomer **T** with its bulky tertiary carbon forms into the spacious $(2\sqrt{7} \times \sqrt{7}) - 2$ lattice with a surface coverage of just 1/7. The plane group of the SAM is $p1$, imparting local organizational chirality to the SAM; there is no global organizational chirality, however, as equal areas of (highly distinct) SAM domains form based upon the two possible spatial orientations of the $(2\sqrt{7} \times \sqrt{7}) - 2$ surface cell. Because of the adsorbate's bulk, adatom-bound motifs cannot be formed and the adsorbates bind to FCC sites of the gold lattice. One binds upright with a $\sim C_3$ axis and thus has achiral binding, the other tips over slightly imparting some chirality but the effect is weak (the lattice is close to $(\sqrt{7} \times \sqrt{7}) - 1$ in which the two molecules have $\sim C_3$ axes)¹⁷ and so this chirality feature is not indicated in Fig. 4. The observed distinct chiral domains arise from the organization of essentially achiral adsorbates.

The linear butanethiol **L** packs tightly into the $(3 \times 2\sqrt{3}) - 4$ lattice at 1/3 coverage. While the adatom complexes take on the racemic *RS* (syn) conformation of the sulfur atoms, chirality is imparted by the internal arrangement of two adatom complexes and a local vacancy into the surface cell. Its plane group is $p1$, a chiral group, but without the local vacancy, a property that little effects the SAM properties, and with a small translation of the adatoms, this would become the achiral cm plane group. Observed STM images do not show distinct chiral domains.¹⁴

Two adatom motifs also pack into the unit cell of the branched chain achiral butanethiol **B** in the $(8 \times \sqrt{3}) - 4$ lattice at an intermediary coverage of 1/4. All four sulfur atoms take on the same chirality but the spacings between the adatom motifs are slightly irregular and so the plane group is $p1$ rather than $p2$. Naively, distinct chiral domains are expected for this butanethiol but the observed STM images assemble spots in a linear fashion along a direction that is $< 5^\circ$ from a lattice vector, making domains difficult to identify.¹⁵⁻¹⁶

In the present work we show that the SAMs of the enantiomerically pure chiral branched-chain butanethiol **C** are very similar to those of **B** except that the two adsorbate complexes per cell in **B** have become translationally equivalent. Syn adatom complexes are produced in both cases but whilst **B** forms equal amounts of domains with *RR* and *SS* configurations, (*R*)-**C** forms a single domain in which the sulfur atoms take on the *SS* configuration while (*S*)-**C** forms a single domain in which the sulfur atoms take

on the *RR* configuration. The SAMs of **C** thus take on both global point chirality and global organizational chirality, the strongest-possible expression of monolayer chirality.¹⁻⁵ However, this expectation is not strongly manifest in the STM images (see e.g. Fig. 1) as the bright and dark spots are oriented parallel to a supercell lattice vector. For example, it is not clear that the domains highlighted by the cyan circle in Fig. 1 are related by reflection symmetry, manifesting global chirality, or just by rotation symmetry. Other properties of these or related SAMs (e.g., catalysis properties of SAM made including substitution of the terminal methyl group) could more significantly reflect the intrinsic chirality, however.

The minor phase **R**₂₅ formed from a racemic mixture of (*R*)-**C** and (*S*)-**C** replaces the two homochiral molecules on each atom with a heterochiral pair without density change, producing an achiral SAM of pg plane-group symmetry. However, the major phase **R**₃₀ shows very complex chirality.¹⁸ The observed STM images take the shape of interleaving stripes each containing 3 adsorbate molecules, with each stripe being the mirror image of the next, implying the achiral pg plane group, but small deviations from this pattern can sometimes be discerned. Interweaving of the $3 \times R$ and $3 \times S$ molecules that fill its $(10 \times \sqrt{3}) - 6$ surface cell increases the coverage from 1/4 for the pure enantiomers and **R**₂₅ to 3/10. This interweaving occurs both through the simultaneous binding of *R* and *S* molecules to each adatom and through the mixing of adatom-bound and surface-bound motifs into the one surface cell. While molecules of **T** take on a circular appearance when directly bonded to Au(111), 2-butanethiol molecules appear elliptical and so bind chirally to the surface. Each surface cell thus contains 12 internal chiral elements, these two plus 5 from each of the adatom complexes. Despite this vast array of chiral binding sites within each surface cell, the overall SAM appears essentially achiral to the STM tip.

5. Conclusions

The butanethiol SAM domains **L**, **B**, **C**, **R**₂₅, **R**₃₀ and **T** manifest chirality on Au(111) in very different ways. The most striking external manifestation found are the distinct domains observed for **T**, but these arise despite the absence of any chiral center within its surface cell. Conversely, **R**₃₀ contains 12 chiral centers per cell but produces an essentially achiral SAM. Further, chiral manifestations of the only system possessing global point chirality and global organizational chirality, **C**, are weakly depicted by STM, as they are for **B**, a molecule with distinct local point chirality;

internal pseudo symmetry planes also essentially destroy chirality for **L**.

Even though the butanethiol family contains the smallest unsubstituted chiral alkanethiol, steric interactions between the ligands rather than the head group always appear to be the dominant factor controlling SAM chirality. The dramatic differences found between enantiomerically pure 2-butanethiol and the major racemate domain **R**₃₀ show how steric packing determines the nature of the head-group interaction, selecting amongst a wide range of possible structural motifs. If adatom motifs are selected then this head group enforces symmetry relationships between two of the adsorbate molecules. Often an anti structure with $\sim C_2$ symmetry results, the most common packing motif found for SAMs made from individual adsorbate molecules not bound together through a mutual head group.² However, this head group also stabilizes the related syn structures with $\sim C_s$ symmetry that are far less common but typically achiral. All surface cells for butanethiol SAMs formed using this head group also have rectangular shape, reducing organizational aspects of chirality, and none of these led to clearly identifiable SAM chiral domains. The fundamental nature of this head group thus has profound influence over the extent to which manifestations of chirality are expressed.

However, when formation of the adatom head-group is sterically inhibited, as observed for tertiary butanethiol, SAMs with readily identifiable chiral domains result. Manipulation of head-group structure can thus be used to influence chiral recognition in alkanethiol SAMs. This manipulation can also be used to control surface pitting as the direct binding of ligands to the Au(111) surface produces regular, pit-free surfaces. Other known SAMs involving direct substrate binding include those of cysteamine (SHCH₂CH₂NH₃⁺) in aqueous solution, for which the tail-group interactions control the SAM structure.⁶⁶⁻⁶⁷ Because of their regularity, SAMs of this type are especially significant for technological applications, and their ability to produce large chiral domains provides another feature of significant interest. Unless the SAM has global point chirality, grain boundaries and defects will always facilitate racemization, however, and so the useful lifetime of the SAM is an issue that would have to be addressed. Our images show locking of asymmetric structures on the STM time-scale but this is very short compared to that expected for a commercially useful material.

ASSOCIATED CONTENT

Supporting Information

Provided are full details of the synthesis, characterization, electrochemistry and STM imaging, as well as full details of the computational methods, energetics, and optimized structures. This material is available free of charge via the Internet at <http://pubs.acs.org>.

AUTHOR INFORMATION

Corresponding Author

Email Jeffrey.Reimers@uts.edu.au, and ju@kemi.dtu.dk.

ACKNOWLEDGMENT

Financial support from the Lundbeck Foundation (R69-A8097) to JZ, the China Scholarship Council and Natural Science Foundation of China (Nos. 20973144 and 21033007) to JY and BM, the Danish Council for Independent Research, Technology and Production Sciences to EA and DT, the EU FP7 Staff Exchange program PIRSES-GA-2012-318990 – ELECTRONANOMAT to

JU, and the Australian Research Council (DP110102932), as well as computational support from National Computational Infrastructure (NCI, D63) to JRR, are gratefully acknowledged.

REFERENCES

- (1) Barlow, S. M.; Raval, R. *Surf. Sci. Rep.* **2003**, *50*, 201.
- (2) Plass, K. E.; Grzesiak, A. L.; Matzger, A. J. *Acc. Chem. Res.* **2007**, *40*, 287.
- (3) Elemans, J. A. A. W.; De Cat, I.; Xu, H.; De Feyter, S. *Chem. Soc. Rev.* **2009**, *38*, 722.
- (4) Slater, A. G.; Beton, P. H.; Champness, N. R. *Chem. Sci.* **2011**, *2*, 1440.
- (5) Ernst, K.-H. *Surf. Sci.* **2013**, *613*, 1.
- (6) Voznyy, O.; Dubowski, J. J.; Yates, J. T.; Maksymovych, P. *J. Am. Chem. Soc.* **2009**, *131*, 12989.
- (7) Guo, Z.; De Cat, I.; Van Averbeke, B.; Ghijsens, E.; Lin, J.; Xu, H.; Wang, G.; Hoeben, F. J. M.; Tomović, Ž.; Lazzaroni, R.; Beljonne, D.; Meijer, E. W.; Schenning, A. P. H. J.; De Feyter, S. *J. Am. Chem. Soc.* **2013**, *135*, 9811.
- (8) Häkkinen, H. *Nat. Chem.* **2012**, *4*, 443.
- (9) Mallat, T.; Orglmeister, E.; Baiker, A. *Chem. Rev.* **2007**, *107*, 4863.
- (10) De Cat, I.; Gobbo, C.; Van Averbeke, B.; Lazzaroni, R.; De Feyter, S.; van Esch, J. *J. Am. Chem. Soc.* **2011**, *133*, 20942.
- (11) Destoop, I.; Xu, H.; Oliveras-Gonzalez, C.; Ghijsens, E.; Amabilino, D. B.; De Feyter, S. *Chem. Commun.* **2013**, *49*, 7477.
- (12) Chaudhuri, A.; Lerotholi, T. J.; Jackson, D. C.; Woodruff, D. P.; Dhanak, V. R. *Surf. Sci.* **2010**, *604*, 227.
- (13) Chaudhuri, A.; Jackson, D. C.; Lerotholi, T. J.; Jones, R. G.; Lee, T. L.; Detlefs, B.; Woodruff, D. P. *Phys. Chem. Chem. Phys.* **2010**, *12*, 3229.
- (14) Wang, Y.; Chi, Q.; Hush, N. S.; Reimers, J. R.; Zhang, J.; Ulstrup, J. *J. Phys. Chem. C* **2011**, *115*, 10630.
- (15) Chi, Q.; Zhang, J.; Ulstrup, J. *J. Phys. Chem. B* **2006**, *110*, 1102.
- (16) Wang, Y.; Chi, Q.; Hush, N. S.; Reimers, J. R.; Zhang, J.; Ulstrup, J. *J. Phys. Chem. C* **2009**, *113*, 19601.
- (17) Wang, Y.; Hush, N. S.; Reimers, J. R. *J. Phys. Chem. C* **2007**, *111*, 10878.
- (18) Ouyang, R.; Yan, J.; Jensen, P. S.; Ascic, E.; Gan, S.; Tanner, D. A.; Mao, B.; Ni, L.; Zhang, J.; Tang, C.; Hush, N. S.; Reimers, J. R.; Ulstrup, J. **2014**, *submitted*.
- (19) Jadzinsky, P. D.; Calero, G.; Ackerson, C. J.; Bushnell, D. A.; Kornberg, R. D. *Science* **2007**, *318*, 430.
- (20) Maksymovych, P.; Sorescu, D. C.; Yates, J. T., Jr. *Phys. Rev. Lett.* **2006**, *97*, 146103.
- (21) Mazzarello, R.; Cossaro, A.; Verdini, A.; Rousseau, R.; Casalis, L.; Danisman, M. F.; Floreano, L.; Scandolo, S.; Morgante, A.; Scoles, G. *Phys. Rev. Lett.* **2007**, *98*, 16102.
- (22) Cossaro, A.; Mazzarello, R.; Rousseau, R.; Casalis, L.; Verdini, A.; Kohlmeyer, A.; Floreano, L.; Scandolo, S.; Morgante, A.; Klein, M. L.; Scoles, G. *Science* **2008**, *321*, 943.
- (23) Nishigaki, J.-i.; Tsunoyama, R.; Tsunoyama, H.; Ichikuni, N.; Yamazoe, S.; Negishi, Y.; Ito, M.; Matsuo, T.; Tamao, K.; Tsukuda, T. *J. Am. Chem. Soc.* **2012**, *134*, 14295.
- (24) Wang, Y.; Hush, N. S.; Reimers, J. R. *J. Am. Chem. Soc.* **2007**, *129*, 14532.
- (25) Grönbeck, H.; Curioni, A.; Andreoni, W. *J. Am. Chem. Soc.* **2000**, *122*, 3839.
- (26) Vargas, M. C.; Giannozzi, P.; Selloni, A.; Scoles, G. *J. Phys. Chem. B* **2001**, *105*, 9509.
- (27) Bilic, A.; Reimers, J. R.; Hush, N. S. *J. Chem. Phys.* **2005**, *122*, 094708.
- (28) Reimers, J. R.; Wang, Y.; Cankurtaran, B. O.; Ford, M. *J. Am. Chem. Soc.* **2010**, *132*, 8378.

- (29) Maksymovych, P.; Sorescu, D. C.; Yates, J. T. *Phys. Rev. Lett.* **2006**, *97*, 146103.
- (30) Sheppard, D. C.; Parkinson, G. S.; Hentz, A.; Window, A. J.; Quinn, P. D.; Woodruff, D. P.; Bailey, P.; Noakes, T. C. Q. *Surf. Sci.* **2011**, *605*, 138.
- (31) Maksymovych, P.; Sorescu, D. C.; Voznyy, O.; Yates, J. T. *J. Am. Chem. Soc.* **2013**, *135*, 4922.
- (32) Poirier, G. E. *Chem. Rev.* **1997**, *97*, 1117.
- (33) Maksymovych, P.; Voznyy, O.; Dougherty, D. B.; Sorescu, D. C.; Yates, J. T., Jr. *Prog. Surf. Sci.* **2010**, *85*, 206.
- (34) Chadha, R. K.; Kumar, R.; Tuck, D. G. *Can. J. Chem.* **1987**, *65*, 1336.
- (35) Paik, W.-k.; Eu, S.; Lee, K.; Chon, S.; Kim, M. *Langmuir* **2000**, *16*, 10198.
- (36) Love, J. C.; Estroff, L. A.; Kriebel, J. K.; Nuzzo, R. G.; Whitesides, G. M. *Chem. Rev.* **2005**, *105*, 1103.
- (37) Widrig, C. A.; Chung, C.; Porter, M. D. *J. Electroanal. Chem. Interfacial Electrochem.* **1991**, *310*, 335.
- (38) Vericat, C.; Vela, M. E.; Benitez, G.; Carro, P.; Salvarezza, R. C. *Chem. Soc. Rev.* **2010**, *39*, 1805.
- (39) Zhong, C.-J.; Woods, N. T.; Dawson, G. B.; Porter, M. D. *Electrochem. Commun.* **1999**, *1*, 17.
- (40) Petroski, J.; Chou, M.; Creutz, C. J. *Organomet. Chem.* **2009**, *694*, 1138.
- (41) Konopka, M.; Rousseau, R.; Stich, I.; Marx, D. *J. Am. Chem. Soc.* **2004**, *126*, 12103.
- (42) Rodriguez, J. A.; Dvorak, J.; Jirsak, T.; Liu, G.; Hrbek, J.; Aray, Y.; Gonzalez, C. *J. Am. Chem. Soc.* **2003**, *125*, 276.
- (43) De, R. V.; Rousseau, R.; Marchetto, D.; Biagi, R.; Scandolo, S.; Del, P. U. *Phys. Rev. Lett.* **2005**, *95*, 046804.
- (44) Chaudhuri, A.; Odellius, M.; Jones, R. G.; Lee, T. L.; Detlefs, B.; Woodruff, D. P. *J. Chem. Phys.* **2009**, *130*, 124708/1.
- (45) Gröenbeck, H. *J. Phys. Chem. C* **2010**, *114*, 15973.
- (46) Zhang, T.; Ma, Z.; Wang, L.; Xi, J.; Shuai, Z. *Philos. Trans. R. Soc., A* **2014**, *372*, 20130018/1.
- (47) Bruening, M.; Cohen, R.; Guillemoles, J. F.; Moav, T.; Libman, J.; Shanzer, A.; Cahen, D. *J. Am. Chem. Soc.* **1997**, *119*, 5720.
- (48) Duwez, A.-S. *J. Elect. Spectrosc. Rel. Phen.* **2004**, *134*, 97.
- (49) Bourg, M.-C.; Badia, A.; Lennox, R. B. *J. Phys. Chem. B* **2000**, *104*, 6562.
- (50) Alloway, D. M.; Hofmann, M.; Smith, D. L.; Gruhn, N. E.; Graham, A. L.; Colorado, R., Jr.; Wysocki, V. H.; Lee, T. R.; Lee, P. A.; Armstrong, N. R. *J. Phys. Chem. B* **2003**, *107*, 11690.
- (51) Howell, S.; Kuila, D.; Kasibhatla, B.; Kubiak, C. P.; Janes, D.; Reifenger, R. *Langmuir* **2002**, *18*, 5120.
- (52) Mendez De Leo, L. P.; de la Llave, E.; Scherlis, D.; Williams, F. J. *J. Chem. Phys.* **2013**, *138*, 114707.
- (53) Zhong, C.-J.; Brush, R. C.; Anderegg, J.; Porter, M. D. *Langmuir* **1998**, *15*, 518.
- (54) Brust, M.; Fink, J.; Bethell, D.; Schiffrin, D. J.; Kiely, C. J. *Chem. Soc., Chem. Commun.* **1995**, 1655.
- (55) Negishi, Y.; Tsukuda, T. *J. Am. Chem. Soc.* **2003**, *125*, 4046.
- (56) Volante, R. P. *Tetrahedron Lett.* **1981**, *22*, 3119.
- (57) Perdew, J. P.; Wang, Y. *Phys. Rev. B* **1992**, *45*, 13244.
- (58) Reimers, J. R.; Panduwinata, D.; Visser, J.; Chin, Y.; Tang, C.; Goerigk, L.; Ford, M. J.; Santic, M.; Sum, T. J.; Coenen, M. J. J.; Elemans, J. A. A. W.; Hush, N. S.; Crossley, M. J. *submitted 2014*.
- (59) Grimme, S.; Antony, J.; Ehrlich, S.; Krieg, H. *J. Chem. Phys.* **2010**, *132*, 154104.
- (60) Kresse, G.; Hafner, J. *Phys. Rev. B* **1993**, *47*, 558.
- (61) Tersoff, J.; Hamann, D. R. *Phys. Rev. Lett.* **1983**, *50*, 1998.
- (62) Molina, L. M.; Hammer, B. *Chem. Phys. Lett.* **2002**, *360*, 264.
- (63) Wang, Y.; Chi, Q.-J.; Zhang, J.-D.; Hush, N. S.; Reimers, J. R.; Ulstrup, J. *J. Am. Chem. Soc.* **2011**, *133*, 14856.
- (64) Wang, J.-g.; Selloni, A. *J. Phys. Chem. C* **2007**, *111*, 12149.
- (65) Luedtke, W. D.; Landman, U. *J. Phys. Chem.* **1996**, *100*, 13323.
- (66) Zhang, J.; Bilic, A.; Reimers, J. R.; Hush, N. S.; Ulstrup, J. *J. Phys. Chem. B* **2005**, *109*, 15355.
- (67) Zhang, J.; Chi, Q.; Nielsen, J. U.; Friis, E. P.; Andersen, J. E. T.; Ulstrup, J. *Langmuir* **2000**, *16*, 7229.

SYNOPSIS TOC

